Donald G. Bodnar
MI Technologies
4500 River Green Parkway, Suite 200
Duluth, Geogia 30096-2580
(678) 475-8317
(678) 475-8391 (Fax)
dbodnar@mi-technologies.com (e-mail)

Echo Identification and Cancellation Techniques for Antenna Measurement in Non-Anechoic Test Sites

Susana Loredo, Marcos R. Pino, Fernando Las-Heras, and Tapan K. Sarkar[1]

Área Teoría de la Señal y Comunicaciones, Dept. Ingeniería Eléctrica, Univ. de Oviedo
Campus de Viesques s/n, Edif. 4, E-33204 Gijón, Spain
E-mail: flasheras@tsc.uniovi.es

[1]Department of Electrical Engineering and Computer Science, Syracuse University
Syracuse, NY 13244-1240 USA
Tel: +1 (315) 443-3775; Fax: +1 (315) 443-4441; E-mail: tksarkar@syr.edu

Abstract

This paper focuses on the measurement of antenna radiation patterns when fully anechoic conditions are not available and, as consequence, some undesirable echoes are initially present in the measure. Two techniques are analyzed and compared, which – starting from data measured in the frequency domain – allow the echo contributions to be identified and the antenna radiation pattern to be retrieved. The accuracy of both techniques is evaluated at the frequency of 22 GHz by comparison with measurements obtained in an anechoic chamber.

Keywords: Anechoic chambers (electromagnetic); antenna measurements; antenna radiation patterns; multipath channels; echo suppression

1. Introduction

In general, the measurement of antenna radiation patterns takes place in anechoic chambers, where one attempts to reduce as much as possible the reflection and diffraction contributions from walls and mechanical devices present inside the chamber. The reduction in the various scattered and diffracted fields is achieved using appropriate absorbing materials. However, the radiation patterns measured in reverberant or semi-anechoic chambers, or even open-area test sites, will certainly present the effects of those undesired components, which will result in inaccuracies in the measured patterns. In those situations, an improvement of the measurements will only be achieved through the removal [1] or compensation [2-4] of the perturbations.

In this paper, two techniques are considered and tested to obtain the radiation pattern of antennas from measurements carried out in reverberant or non-anechoic conditions. For this purpose, a metal plate has been introduced inside an anechoic chamber, which will introduce contributions due to the reflected and diffracted components of the fields in the measurements. The goal of this

paper is to describe a methodology that will reduce these unwanted components, and that will eliminate them from the measurements in order to obtain a radiation pattern as similar as possible to the one obtained in an anechoic chamber.

The first technique to be described estimates the impulse response of the reverberant chamber from its frequency response by using the inverse Fourier transform. In the time domain, the direct contribution is detected and gated, eliminating the undesired echoes. Applying the Fourier transform to this new time response where only the direct contribution is present, the radiation pattern can be retrieved at the frequency of interest. The second technique is based on the Matrix-Pencil Method [5], used to approximate signals into a sum of complex exponentials. This method has been successfully applied to several electromagnetic problems [6, 7]. In particular, the Matrix-Pencil Method has been also applied in [1] to reconstruct the frequency response of antennas measured in a semi-anechoic chamber by identification and elimination of the ground-reflected components.

The measurement system and the procedure used to obtain the data are described in Section 2. The two techniques introduced above, based on the Fourier transform and Matrix-Pencil algorithms, are described in Sections 3 and 4, respectively, as well as their application to the data measured in the reverberant chamber. Sample processed results are presented in Section 5, and compared to the data measured in a fully anechoic chamber. Finally, Section 6 summarizes the conclusions that have been derived from this work, and presents a methodology for an automatic implementation of the proposed techniques.

2. Measurement System

All the measurements presented in this paper were obtained using the near-field/far-field spherical-range measurement system in an anechoic chamber (8 m × 5 m × 4.5 m) located in the ANTEM Lab (Antennas and Electromagnetic Emissions Measurement Laboratory) at the University of Oviedo, designed to operate at frequencies ranging from 1 GHz to 40 GHz. Figure 1 shows both the antenna under test (AUT), mounted on a rollover azimuth-positioning system, and the probe, mounted on a polarization positioner. A simplified scheme of the whole measurement system is also included in Figure 2. For these experiments, the probe and the AUT were selected to be identical pyramidal-horn antennas, with an approximately constant gain of 20 dB in the frequency band between 17.7 GHz and 26.7 GHz. They were placed at a height of 2 m above ground level, and separated from each other by 5.4 m (396 wavelengths at the frequency of 22 GHz) during the whole measurement campaign. The system controlling the positioners allowed the setting of the azimuth and roll orientation of the AUT, as well as the polarization of the probe, via software.

In order to compensate for the signal attenuation along the different RF coaxial cables, two amplifiers were used in the measurement system, one in the transmission path and another one in the reception section, both operating in the 18 GHz to 26 GHz band, with a typical gain of 28 dB. After the transmission amplifier, a directional coupler was inserted to get a reference of the signal radiated by the antenna. Finally, a Rohde-Schwarz ZVK vector network analyzer was used as transmitter-receiver equipment.

In this anechoic environment, the necessary reference data were taken: the azimuth (ϕ) radiation pattern of the AUT between

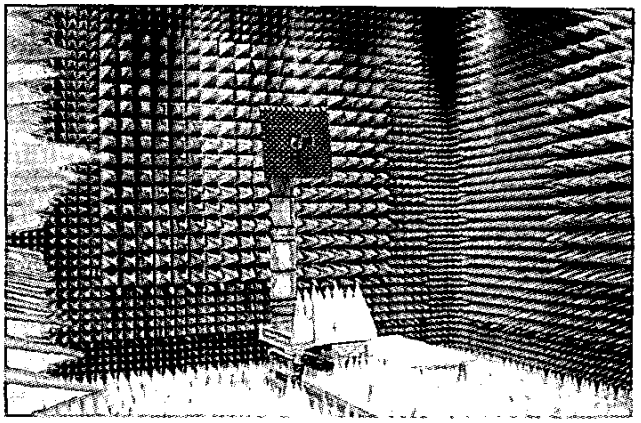

Figure 1a. An anechoic chamber in ANTEM-LAB, with the AUT on a rollover azimuth positioner.

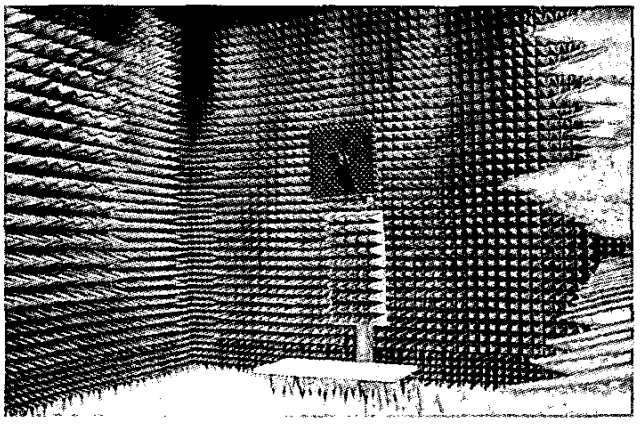

Figure 1b. An anechoic chamber in ANTEM-LAB, with the probe on a polarization positioner.

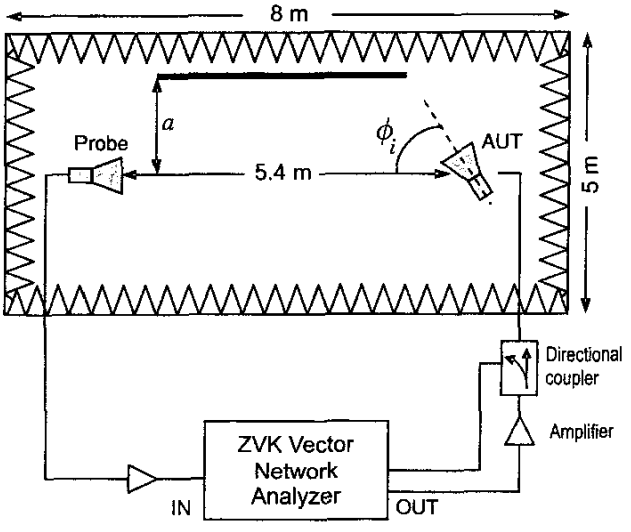

Figure 2. A top view of the antenna-measurement scheme. The copper plate has been introduced into the anechoic chamber to model a reverberant chamber.

0° and 90° at the frequency of 22 GHz for an elevation angle (θ) equal to zero degrees. This information is used in Section 5 to validate the results obtained by using both the techniques to be described. Once the reference measurement was obtained, a 2 m × 1 m rectangular copper plate was placed inside the anechoic chamber, in order to simulate a partially reverberant chamber. This is shown in Figure 2, where the separation between the plate and the antennas' line-of-sight (parameter a) could be configured for the different measurements, generating different scenarios or situations that had to be separately analyzed.

The measurement campaign was carried out in the frequency domain, measuring the $S_{21}(f)$ parameter of the system in the band of interest (18 to 26 GHz, 22 GHz the center frequency of the band) for each azimuth angle of radiation, ϕ_i, ranging from 0° to 90° in steps of 0.5°. Thus, for each step of the azimuth positioner, the channel transfer function around 22 GHz was measured. The process was repeated for each position of the copper plate. Considering that one of the two techniques is based on the Fourier transform, and bearing in mind the relationships that this algorithm establishes between the frequency domain and the time domain, the bandwidth (BW), the time resolution (Δt), and the step (Δf) of the frequency sweep must be carefully chosen. These parameters will be established as functions of the time delay (δt) from the arrival of the direct contribution until the arrival of the reflected or diffracted contributions (multipath components). This time delay, which is an indication of the minimum time resolution (Δt) required for ulterior processing in the time domain, will depend on the separation between the antennas and the location of the obstacles causing the undesirable received components. Therefore, the minimum bandwidth required for the frequency sweep can be directly obtained as the reciprocal of the time delay, i.e., $BW = 1/\delta t$. However, it is advisable to use a higher time resolution to better distinguish the different contributions in the time domain. For this reason, a larger bandwidth, of approximately $10/\delta t$, has been used in these measurements. On the other hand, the frequency step, Δf, is chosen as a function of the time-response length, again taking into account the distance between the antennas and the location of the main reflecting/diffracting elements located inside the chamber.

Once the parameters of the frequency sweep have been selected, the measurement procedure is straightforward and very fast. As commented above, for each azimuth angle of the AUT, a measure of the S_{21} parameter, relating the input and output ports of the vector network analyzer, is done for the whole frequency range. The frequency sweep performed by the analyzer is fast, and it takes just a few seconds to obtain the response $S_{21}(f,\phi_i)$ for a large number of frequencies. After performing the whole azimuth sweep, the results are stored in a matrix, $S_{21}(f,\phi)$, which is the starting point for the analysis detailed in the following sections.

3. FFT-Based Method

It is well known that in an ideal situation, the only path that exists between the AUT and the probe is the direct propagation path. The radio channel in the frequency domain is then characterized by a constant amplitude response, independent of the frequency, and a linear phase. However, considering multipath propagation, the above is not true anymore, and frequency-selective fading may appear, showing the influence of the echo contributions both in the amplitude and the phase of the channel frequency response. The measure of the channel frequency response is a process widely used to estimate the impulse response or time response of the multipath propagation channel [8-10]. Once in the time domain, it is relatively easy to identify those multipath components and to estimate the channel impulse response in anechoic conditions. This is the idea that inspires the technique that has been called the "FFT-Based Method."

Figure 3 illustrates the different steps to be followed when applying this technique to the data previously measured for a given location of the copper plate. First, the measured coherent (amplitude/phase) frequency response, $S_{21}(f,\phi)$, shown in Figure 3a, is windowed using a Hanning window (Figure 3b) before applying the inverse FFT to obtain the time-domain response of the system, $S_{21}(t,\phi)$. The windowing of the raw data turns out to have a slightly worse time resolution, which will now be the reciprocal of the bandwidth swept multiplied by the width of the window used. This can be particularly relevant in the case of a very short time delay between the main and the echo components. Bearing this in mind, as well as the level of the secondary lobes of the different windows commonly used, the Hanning window was finally chosen since it shows a good compromise between the reduction of the sidelobe level and the widening of the main lobe [11]. It can be observed in Figures 3a and 3b that the propagation channel between the two antennas is almost ideal for azimuth angles in the range between 0° and 20°. For that orientation of the AUT, the wave that impinges on the metal plate is radiated through a secondary lobe and, consequently, with a very low power level. However, for higher angles, the frequency-selective fading starts being evident, as the main beam of the AUT points at the reflection point on the metal plate.

Once in the time domain, Figure 3c, the direct contribution is detected and gated, eliminating the delayed response due to the reflected and diffracted components. This results in an impulse response $S'_{21}(t,\phi)$, shown in Figure 3d, comparable to the impulse response measured in an anechoic situation.

Returning to the frequency domain by means of the application of the FFT algorithm to $S'_{21}(t,\phi)$, the antenna radiation pattern at the central frequency, f_c, is obtained as $S'_{21}(f_c,\phi)$. This should be similar to the response obtained in a fully anechoic chamber. The comparison between the AUT pattern measured in this way and the reference measurement (in anechoic conditions) is included in Section 5, Figure 5.

4. Matrix-Pencil Method

The second technique tested in this paper is based on the Matrix-Pencil Method (MPM) [5]. The Matrix-Pencil technique is used to approximate functions as sums of complex exponentials. The technique tested here includes the use of the Matrix-Pencil Method to obtain an approximation of the chamber response (in terms of the $S_{21}(f)$ parameter) as a sum of exponential terms. This approximation is applied to the $S_{21}(f)$ measured data in the frequency domain so the complex exponentials can be directly related to the different contributions arriving at the probe (direct, reflected, and diffracted components) [1]. The $S_{21}(f)$ response obtained for a given frequency range will be decomposed as

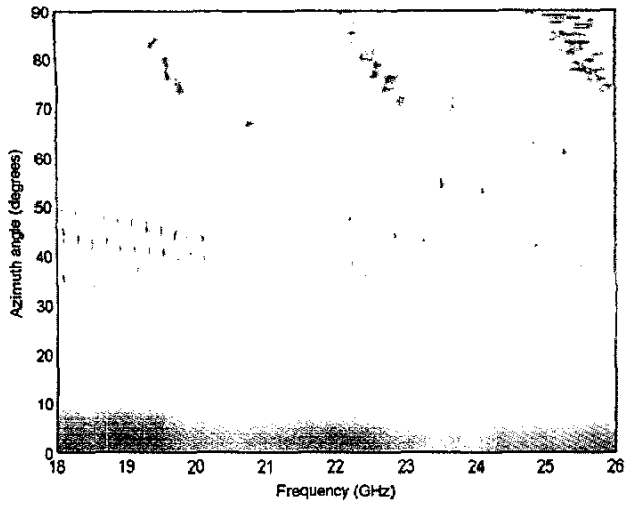

Figure 3a. The steps followed in the FFT-Based Method: $S_{21}(f,\phi)$, the channel frequency response (18-26 GHz) for each azimuth angle (0°-90°).

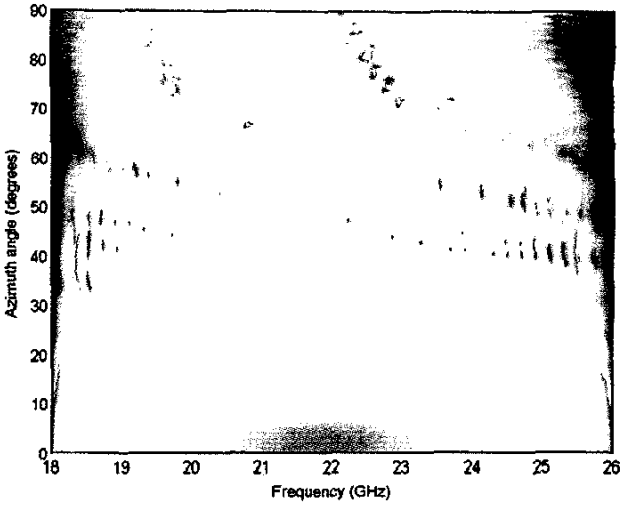

Figure 3b. The steps followed in the FFT-Based Method: $S_{21}(f,\phi)$ multiplied by the Hanning window.

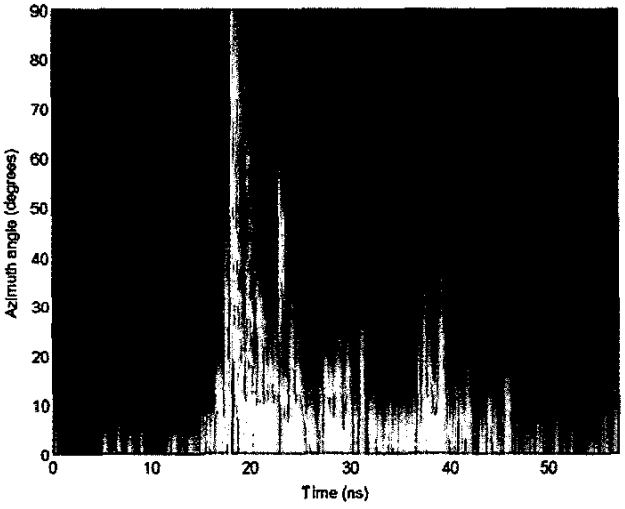

Figure 3c. The steps followed in the FFT-Based Method: $S_{21}(t,\phi)$, the time response for each azimuth angle.

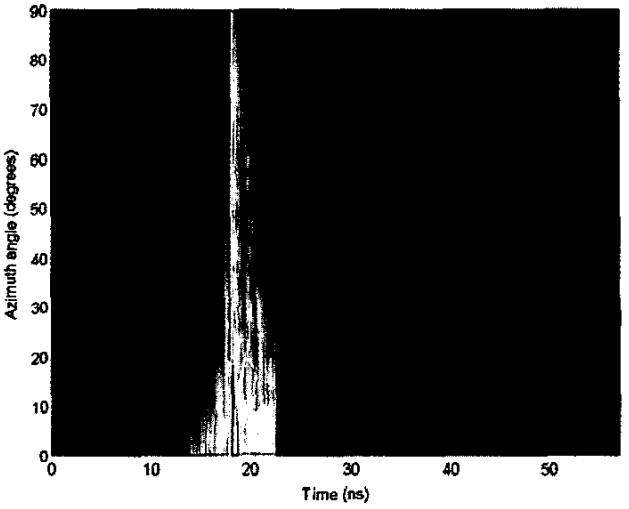

Figure 3d. The steps followed in the FFT-Based Method: $S'_{21}(t,\phi)$, the time response after elimination of delayed components.

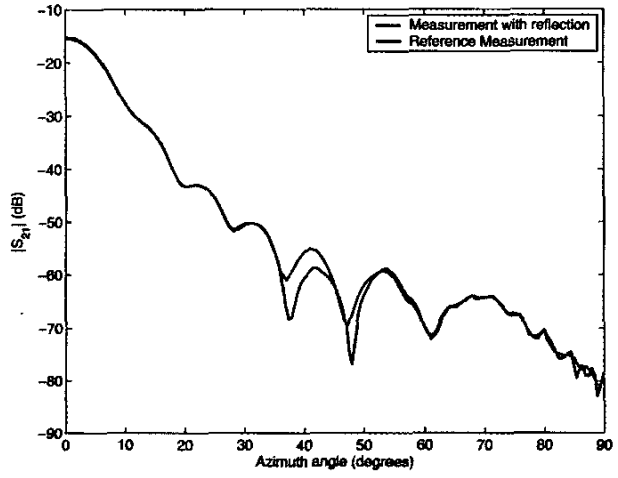

Figure 4. Example 1, $a = 2.05$ m: The radiation pattern measured in reverberant conditions.

$$S_{21}(f) = \sum_{m=1}^{M} R_m e^{s_m f} . \quad (1)$$

Once the $S_{21}(f)$ response is modeled as a combination of different complex exponentials, the next step is to determine which term corresponds to the direct contribution, so the other contributions (reflections, diffractions) can be suppressed from the measured data. The chamber response in anechoic conditions will then be obtained. The detailed procedure is explained next.

The procedure starts with the measured data, $S_{21}(f,\phi)$, obtained as described in Section 5. The measurements are performed for different azimuth angles ϕ_i and, for each azimuth angle, a set of data for different frequencies between f_0 and f_{N-1} is measured at intervals of Δf ($f_k = f_0 + k\Delta f$). The Matrix-Pencil Method is now applied to the measured data in order to model the frequency response of $S_{21}(f)$ for each one of the azimuth angles. Then, as in [7], the $S_{21}(f)$ response for the azimuth angle ϕ_i can be expressed as

$$S_{21}(f_k)\big|_{\phi_i} = \sum_{m=1}^{M} R_m e^{s_{m,i} k\Delta f} = \sum_{m=1}^{M} R_{m,i} z_{m,i}^{k} \quad \forall k = 0,...,N-1 , \quad (2)$$

where M is the number of complex exponentials used in the approach, and $s_{m,i}$ and $R_{m,i}$ are the coefficients given by the Matrix-Pencil Method corresponding to the mth complex exponential term for the ith angle. The $s_{m,i}$ coefficients provide information about the propagation of each contribution in terms of attenuation and time delay, while the $R_{m,i}$ are the amplitudes of each exponential term. The procedure for obtaining those coefficients is as follows. First, a Hankel matrix, $[Y]$, is formed with the sample data $S_{21}(f_k)\big|_{\phi_i}$,

$$[Y] = \begin{bmatrix} S_{21}(f_0)\big|_{\phi_i} & S_{21}(f_1)\big|_{\phi_i} & \cdots & S_{21}(f_L)\big|_{\phi_i} \\ S_{21}(f_1)\big|_{\phi_i} & S_{21}(f_2)\big|_{\phi_i} & \cdots & S_{21}(f_{L+1})\big|_{\phi_i} \\ \vdots & \vdots & \ddots & \vdots \\ S_{21}(f_{N-L-1})\big|_{\phi_i} & S_{21}(f_{N-L})\big|_{\phi_i} & \cdots & S_{21}(f_{N-1})\big|_{\phi_i} \end{bmatrix}_{(N-L)(L+1)} \quad (3)$$

where L is referred to as the pencil parameter [5]. Then, the $z_{m,i}$ terms are obtained as the eigenvalues of $[V_2]^{\perp}[V_1]$, where the matrices $[V_1]$ and $[V_2]$ are obtained by truncating the M first rows of the $[V]$ matrix that results from the singular-value decomposition (SVD) of $[Y] = [U][\Sigma][V]^T$, and suppressing the first and last columns, respectively ($[V_2]^{\perp}$ stands for the pseudoinverse of $[V_2]$) [7]. Finally, the complex amplitude coefficients, $R_{m,i}$, are obtained by solving a least-square problem:

$$S_{21}(f_k)\big|_{\phi_i} = \sum_{m=1}^{M} \left(e^{s_{m,i}\Delta f}\right)^k R_{m,i} , \quad \forall k = 0,...,N-1 . \quad (4)$$

Once the Matrix-Pencil Method is applied to the S_{21} data, an expression similar to Equation (2) is obtained for each measured azimuth angle. In order to reconstruct the radiation pattern of the AUT in anechoic conditions, it is necessary to determine the complex exponential that models the direct-contribution propagation for each azimuth angle. For that purpose, the information about the attenuation and delay of the propagation of the different contributions arriving at the probe, provided by the complex coefficients $s_{m,i}$, is used. Considering that the propagation delay of the direct contribution should remain constant for all the azimuth angles, this delay can be easily obtained for the azimuth angle $\phi_0 = 0°$. For this azimuth angle, the direct-contribution amplitude ($R_{d,0}$ coefficient) must be greater than the amplitudes of the rest of the exponential terms $R_{i,0}$. Once the direct contribution term is identified for ϕ_0, the direct contributions for the rest of the azimuth angles are determined by comparing their propagation delay with that obtained at ϕ_0.

Then, the radiation pattern of the AUT at the central frequency $f_c = f_k$ (with $k = (N+1)/2$) in full anechoic conditions can be approximated in terms of an amplitude and a complex exponential for each azimuth angle:

$$S_{21}(f_c,\phi) = R_{d,i} e^{s_{d,i} c\Delta f} . \quad (5)$$

Finally, some considerations followed for the practical implementation of the Matrix-Pencil Method are presented. First, an order of $M = 3$ or $M = 4$ yields accurate modeling of the direct and reflected contributions, as well as other contributions due to diffractions in the plate edges and/or in the structures supporting the antennas. The frequency bandwidth needed for a good approximation of the Matrix-Pencil Method has been determined following [1], and corresponds to one cycle of the interference between the direct ray and the reflected ray. This bandwidth can be directly related to the time delay of the reflected contribution by $1/\delta t$. For a given frequency f_c, the frequency sweep for the Matrix-Pencil Method should cover from $f_c - 1/(2\delta t)$ to $f_c + 1/(2\delta t)$.

5. Measurements and Results

Two examples, corresponding to two different locations of the copper plate, are presented and analyzed in this section, in order to verify the accuracy of the procedures described in Sections 3 and 4. The frequency of 22 GHz, as commented above, was chosen to obtain the radiation pattern of the horn antenna under test.

In the first example, the distance, a, from the plate to the antennas' line-of-sight was 2.05 m. In this situation, the main effects produced by the copper plate on the antenna pattern were expected when the azimuth position of the AUT ranged approximately from 30° to 50°, with the main beam of the antenna pointing directly at the plate, as had already been appreciated in Figure 3a. The time delay (δt) of the component reflected on the plate in relation to the time of arrival of the direct contribution can be easily estimated according to the specular reflection law, and was expected to be about 4.7 nsec. With this estimate, and bearing in mind the comments in Section 2, a bandwidth of 8 GHz was chosen, thus achieving an approximate time resolution of $\Delta t = \delta t/36$ (before windowing the frequency response). A frequency step, Δt, of 5 MHz provided a time response long enough

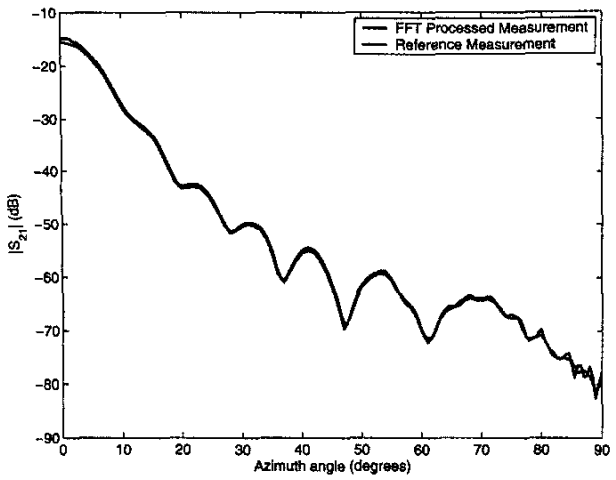

Figure 5. Example 1, $a = 2.05$ m: A comparison between the processed result using the Fourier-Transform Method and the reference measurement.

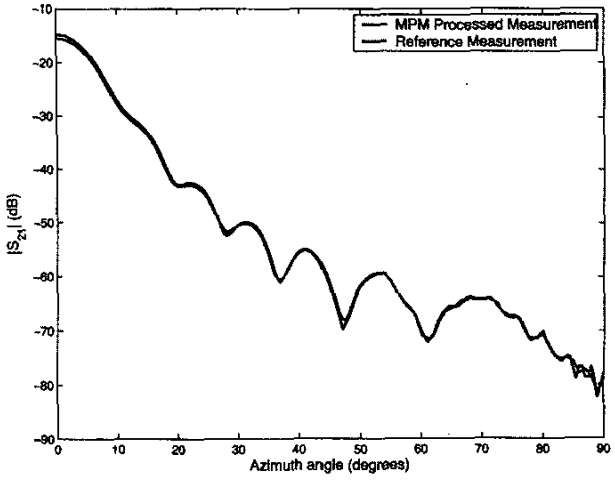

Figure 6. Example 1, $a = 2.05$ m: A comparison between the processed result using the Matrix-Pencil Method and the reference measurement.

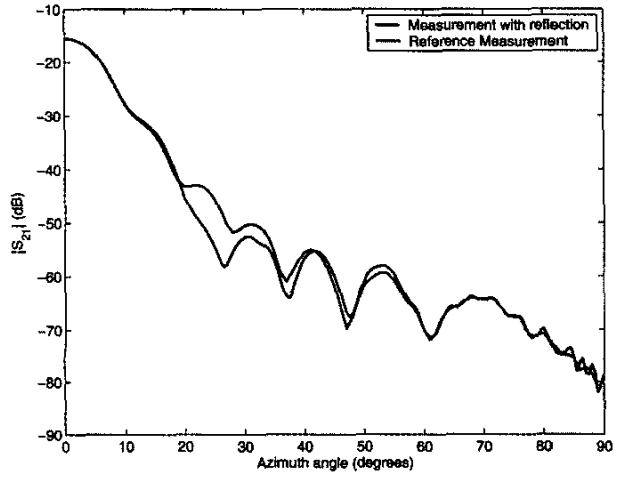

Figure 7. Example 2, $a = 1$ m: The radiation pattern measured in reverberant conditions.

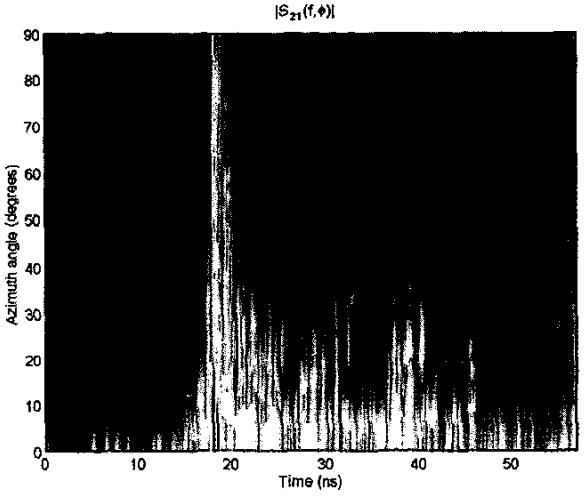

Figure 8. Example 2, $a = 1$ m: The time response as a function of azimuth angle.

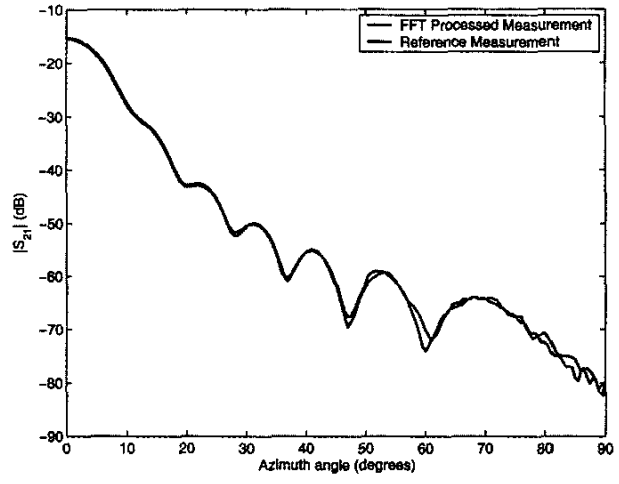

Figure 9. Example 2, $a = 1$ m: A comparison between the processed result using the Fourier-Transform Method and the reference measurement.

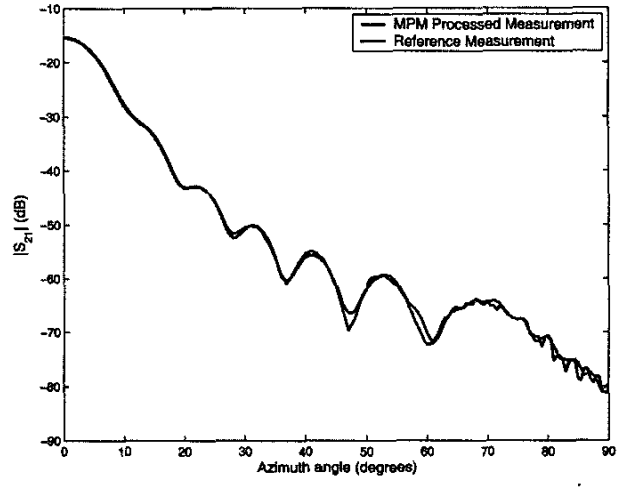

Figure 10. Example 2, $a = 1$ m: A comparison between the processed result using the Matrix-Pencil Method and the reference measurement.

Table 1. The error levels obtained for the processed results using both techniques.

Error	Example 1		Example 2	
	FFT	MPM	FFT	MPM
Mean Error Level (dB)	0.58	0.49	0.62	0.56
STD Error Level (dB)	0.30	0.36	0.72	0.67
Maximum Error Value (dB)	2.05	1.87	3.91	3.03

to avoid aliasing among the most important contributions, giving a total of 1601 frequency samples for each azimuth position. Therefore, the size of the matrix, $S_{21}(f,\phi)$, measured for each situation was be 1601 rows by 801 columns.

Figure 4 compares the radiation pattern measured for this position of the metal plate with the reference pattern measured in the fully anechoic chamber. It can be observed that the presence of the plate certainly affected the radiation pattern, mainly for azimuth angles in the range from 30° to 50°, as had been foreseen.

The time response of the S_{21} parameter as a function of the azimuth angle is the one shown in Figure 3c. The presence of the direct contribution can be noticed at all angles, with a propagation time of approximately 18 nsec and an amplitude that decreased as the azimuth angle increased, due to radiation by lower secondary lobes. The delayed contribution due to reflection on the metal plate is noticeable at the estimated delay of about 4.7 nsec, with a higher amplitude in the range of angles already observed in Figure 4, i.e., between 30° and 50°. For the lowest azimuth angles, mainly between 0° and 10°, some other less important echoes appeared, which can be attributed to small reflections produced in the structures that supported the antennas. Following with the FFT-Based Method, the elimination of all the contributions with a propagation time greater than 22 nsec guarantied that all the effects due to the metallic plate disappeared. The length of the $S'_{21}(t,\phi)$ time response was then determined by detecting the direct component, and considering the widening of the time-domain impulses due to the Hanning window used.

Transforming this modified time response (shown in Figure 3d) back to the frequency domain, and plotting the azimuth variation of S'_{21} at the frequency of 22 GHz, i.e., $S'_{21}(22\,\text{GHz},\phi)$, a radiation pattern similar to the one obtained in an anechoic chamber was achieved. This can be checked in Figure 5, which shows the comparison between the reference measurement taken under anechoic conditions and the result obtained when the measurement in reverberant conditions was processed with the method based on the FFT algorithm. The resemblance between both the curves is evident, and has been quantified by the mean value of the error (0.58 dB), defined as the absolute value of the difference between the curves, and the standard deviation of that error (0.30 dB). The maximum value of the error was 2.05 dB, corresponding to the highest azimuth angles, around 90°, where the received signal levels were much lower than those of the main lobe, and consequently a certain lack of precision can be attributed to the measurement equipment itself. These error values, together with those corresponding to the rest of the analyzed situations, are summarized in Table 1.

To apply the Matrix-Pencil technique to the measured data in this example, the first step was to determine the frequency sweep needed for this method, as described in Section 4. In this case, the estimated delay between the direct contribution and the reflected contribution was about 4.7 nsec, so the frequency bandwidth was established around 200 MHz. A total of 51 samples, from $f_0 = 21.875\,\text{GHz}$ to $f_{N-1} = 22.125\,\text{GHz}$ and an order of $M = 3$ were set as inputs to the Matrix-Pencil Method. The radiation pattern obtained by processing the $S_{21}(f,\phi)$ data with the Matrix-Pencil Method is shown in Figure 6. In this figure, a comparison between the reference radiation pattern and the radiation pattern reconstructed with the Matrix-Pencil Method is plotted. It can be seen that there is excellent agreement between both radiation patterns, the error being quantified by a mean of 0.49 dB, a standard deviation of 0.36 dB, and a maximum value of 1.87 dB.

In the second example, the metal plate was located closer to the antennas, with $a = 1$ m. This situation presented a more important interaction between the antennas and the metal plate, noticeable over a wider range of azimuth angles, as shown in Figure 7. Figure 7 compares the AUT azimuthal patterns measured with and without the metal plate inside the anechoic chamber. Now, the range of azimuth angles where the pattern was evidently distorted extended from 20° to about 60°.

In this situation, the estimated delay for the contribution reflected in the metal plate was 1.2 nsec. Therefore, using the same bandwidth and frequency sweep as in the previous example, a time resolution of $\delta t/10$ was obtained. Figure 8 shows the time response for this new situation, where the presence of the delayed component immediately after the main path is noticeable in a wide range of azimuth angles. In this case, when applying the method based on the Fourier transform algorithm, all the echoes with a delay greater than 1 nsec were eliminated. The FFT was performed on this modified time response, and the radiation pattern obtained at the frequency of 22 GHz again presented good agreement with the reference pattern obtained in anechoic conditions. The comparison between both patterns is presented in Figure 9. The mean error of the estimated pattern was 0.62 dB and the standard deviation of the error was 0.72 dB, the maximum error having reached a value of 3.91 dB.

Finally, the Matrix-Pencil Method was applied to the data measured in the second configuration. In this case, the beat frequency between the direct and reflected rays was lower than in the previous example, so the number of data samples needed for the Matrix-Pencil Method was larger. This meant that the bandwidth of $S_{21}(f,\phi)$ had to be increased up to 800 MHz, from $f_0 = 21.6\,\text{GHz}$ to $f_{N-1} = 22.4\,\text{GHz}$, with a total of 151 samples (keeping the Δf used in the previous example). Figure 10 shows a comparison between the reconstructed radiation pattern and the reference pattern (measured in anechoic conditions), using three exponential terms ($M = 3$) to model the $S_{21}(f,\phi)$ for each azimuth angle. As a reference of the agreement between both results, the mean error level was 0.56 dB with a standard deviation of 0.67 dB, while the maximum error level was 3.3 dB.

6. Conclusions

In this paper, two different techniques have been used to obtain the radiation pattern of antennas from measurements obtained in non-anechoic sites. One technique is based on the Fourier transform, and the other is based on the Matrix-Pencil Method. Different situations have been considered, checking how these techniques deal with echoes from nearby objects where the time delay between the direct contribution and the reflected/diffracted

contributions is only a few nanoseconds. The accuracy of these techniques has been evaluated, showing examples of how the reflections and diffractions from metallic walls and objects can be suppressed. The comparison of the processed patterns with the patterns measured in an anechoic chamber has shown that the mean error of the estimations was less than 0.7 dB, and that both techniques exhibited similar behavior. Meanwhile, the maximum error found was 3.9 dB, appearing at azimuth angles where the level of the radiation pattern was below −70 dB. From the results presented in the previous section, both techniques showed very good agreement with the reference pattern measured in anechoic conditions, even in the scenario where the metal plate was separated 1 m from the antennas. This last situation was more critical, considering that the time delay between the direct contribution and the reflected contribution was only 1.2 nsec.

Both techniques require performing measurements in a frequency range, even though the Matrix Pencil Method requires a smaller bandwidth than the FFT-based technique. Another important consideration is that the accuracy of the FFT technique is more dependent on the parameters (Δf and BW) that define the frequency sweep. The higher the bandwidth, the more accurate are the results obtained in the time domain, although it has been checked that a time resolution Δt (before windowing) of approximately $\delta t/5$ is enough to obtain satisfactory results. For that resolution, the error values found were very similar to those obtained for the highest resolutions analyzed in this paper. In Example 1, a mean error and standard deviation of 0.60 dB and 0.29 dB, respectively, were found, while the maximum value of the error was 1.79 dB. In Example 2, the mean error, standard deviation, and the maximum error were, respectively, 0.69 dB, 0.65 dB, and 3.12 dB. On the other hand, the Matrix Pencil Method is quite dependent on the parameter, M, that defines the number of exponentials used in the expansion of Equation (1). The value of M may vary under noisy conditions and may affect the accuracy of the method.

Finally, some considerations must be taken into account for a practical application of these techniques. First, under the aim of developing an automatic algorithm for both techniques, a good characterization of the measurement chamber must be done. The main purpose is to determine or estimate the time delay, δt, of the first echo arriving at the probe after the direct contribution, since this value will allow one to set up the different input parameters of both techniques (bandwidths and time resolution). The other considerations have to do with the characteristics of the different components of the measured process: depending on the amplifiers' bandwidths and/or the AUT and the frequency bands of the probe, some frequency sweeps cannot be performed under the same conditions, i.e., the components do not present constant gain in the selected band, which may result in an erroneous solution for the reconstruction of the pattern in an anechoic-chamber environment.

7. Acknowledgement

This work was supported by the Spanish "MCYT – Ramón y Cajal" program under projects CAJAL-01-14 and CAJAL-01-15, and the CICYT TIC2002-02391 and FICYT PC-TIC01-08 projects.

8. References

1. B. Fouresté, Z. Altman, J. Wiart, and A. Azoulay, "On the Use of the Matrix-Pencil Method to Correlate Measurements at Different Test Sites," *IEEE Transactions on Antennas and Propagation*, **AP-47**, 10, October 1999, pp. 1569-1573.

2. D. N. Black and E. B. Joy, "Test Zone Field Compensation," *IEEE Transactions on Antennas and Propagation*, **AP-43**, 4, April 1995, pp. 362-368.

3. D. A. Leatherwood and E. B. Joy, "Plane Wave, Pattern Subtraction, Range Compensation," *IEEE Transactions on Antennas and Propagation*, **AP-49**, 12, December 2001, pp. 1843-1851.

4. P. S. H. Leather and D. Parsons, "Equalization for Antenna-Pattern Measurements: Established Technique – New Application," *IEEE Antennas and Propagation Magazine*, **45**, 2, April 2003, pp. 154-161.

5. T. K. Sarkar and O. Pereira, "Using the Matrix Pencil Method to Estimate the Parameters of a Sum of Complex Exponentials", *IEEE Antennas and Propagation Magazine*, **37**, 1, February 1995, pp. 48-55.

6. Y. Hua, and T. K. Sarkar, "Generalized Pencil-of-Function Method for Extracting Poles of an EM System from its Transient Response," *IEEE Transactions on Antennas and Propagation*, **AP-37**, 2, February 1989, pp. 229-234.

7. R. S. Adve, T. K. Sarkar, O. Pereira-Filho, and S. M. Rao, "Extrapolation of Time-Domain Responses from Three-Dimensional Conducting Objects Utilizing the Matrix Pencil Technique," *IEEE Transactions on Antennas and Propagation*, **AP-45**, 1, January 1997, pp. 147-156.

8. S. J. Howard and K. Palahvan, "Measurement and Analysis of the Indoor Radio Channel in the Frequency Domain," *IEEE Transactions on Instrumentation and Measurement*, **IM-39**, 5, October 1990, pp. 751-754.

9. H. Zaghoul, G. Morrison, and M. Fattouche, "Frequency Response and Path Loss Measurements of Indoor Channel," *Electronics Letters*, **27**, 12, June 1991, pp. 1021-1022.

10. S. Loredo, L. Valle, R. P. Torres, "Accuracy Analysis of GO/UTD Radio-Channel Modeling in Indoor Scenarios at 1.8 and 2.5 GHz," *IEEE Antennas and Propagation Magazine*, **43**, 5, October 2001, pp. 37-51.

11. f. j. harris, "On the Use of Windows for Harmonic Analysis with the Discrete Fourier Transform," *Proceedings of the IEEE*, **66**, 1, January 1978, pp. 51-84.